

Doctoral Dissertation (Censored)

博士論文（要約）

Study on Iron and Zinc Dithiolene 2-D Coordination
Frameworks and Lateral Heterojunctions Produced by
Transmetallation

(鉄および亜鉛ジチオレンの2次元錯体フレームワークと
トランスメタル化により作製したヘテロ接合体の研究)

A Dissertation Submitted for the Degree of Doctor of Philosophy
December 2019

令和元年 12 月 博士（理学）申請

Department of Chemistry, Graduate School of Science,
The University of Tokyo

東京大学大学院理学系研究科

化学専攻

陳俊銘

Tan Choon Meng

Abstract

This thesis describes the fabrication strategy towards two-dimensional metalladithiolene coordination nanosheets utilizing zinc (II) and Fe (II) ions. I have demonstrated that it is possible to obtain zinc dithiolene (ZnBHT) and iron dithiolene (FeBHT) nanosheets with defined morphology and crystalline structure. Post-synthetic modification of ZnBHT by transmetallation with other metal ions was explored. In addition, area-specific transmetallation of ZnBHT with 2 different metal ions gives lateral heterojunctions.

Chapter 1 introduces the background of 2-dimensional frameworks. I will discuss the current research on 2D materials leading towards metal-organic frameworks and coordination nanosheets with dithiolene chemistry.

Chapter 2 investigates the synthesis and characterization of ZnBHT. The sheet has been characterized using XPS, SEM, HR-TEM, IR spectroscopy and AFM. The structure of ZnBHT nanosheet is also elucidated by PXRD studies.

Chapter 3 describes the synthesis of iron (II) dithiolene nanosheet (FeBHT-H). FeBHT-H was synthesized using a heated liquid-liquid interfacial method and characterized with various techniques such as IR spectroscopy, XPS, SEM and TEM. Electrical properties were also measured and compared with those of FeBHT synthesized at room temperature.

Chapter 4 details a method developed for production of thin and large area ZnDT which facilitates complete transmetallation. The area-specific transmetallation process is described and the resulting transmetallated metalladithiolene (tmMDT) nanosheets characterized. Electrical conductivity of the tmMDT sheets were measured and compared.

Chapter 5 shows the area-specific transmetallation of ZnDT with two different metal ions, giving lateral heterojunctions consisting of two different metalladithiolene nanosheets. 3 metal ions were used (Ni^{2+} , Cu^{2+} , Fe^{2+}) giving 3 combination-pairs of lateral heterojunctions. The electrical properties of these heterojunctions were measured and discussed. Rectifying behavior was observed in the tmCuDT-tmFeDT lateral heterojunction.

Chapter 6 concludes the present study and gives the future prospective on this coordination framework research.

Contents

Abstract

Chapter 1 General introduction

1.1. Introduction: Two-Dimensional Materials	1
1.1.1 Graphene	2
1.1.2. Layered Metal Hydroxides	3
1.1.3. Transition Metal Dichalcogenides	4
1.1.4. Surface Covalent Organic Frameworks	5
1.1.5. Metal Organic Coordination Nanosheets (CONASHs)	6
1.2. Fabricating Nanosheets – Approaches	
1.2.1. Top-down approach	
1.2.2. Bottom-up approach	7
1.3. Dithiolene Chemistry	8
1.4. CONASHs using Benzenhexathiol (BHT) ligand	9
1.5. Thesis Outline	10
1.6. References	10

Chapter 2 Bisdithiolatozinc(II) Coordination Nanosheets

2.1. Introduction	14
2.1.1 Rationale of Research	16
2.2. Liquid-liquid Interfacial Synthesis of ZnBHT	16
2.3. Characterization of ZnBHT	
2.3.1. Atomic Force Microscopy	17
2.3.2. Scanning Electron Microscopy	18
2.3.3. High Resolution Transmission Electron Microscopy	19
2.3.4. Powder X-ray Diffraction and Simulations	19
2.3.5. X-ray Photoelectron Spectroscopy	24
2.3.6. Infrared Spectroscopy	26
2.3.7. Cyclic voltammetry	26
2.3.8. Exfoliation of ZnBHT nanosheets	27
2.4. Effect of changing solvent systems on ZnBHT-H structure	29

2.5. Effect of changing Zn salt on ZnBHT-H structure	30
2.6. Conclusion	
2.7. Experimental Method	31
2.7.1. Liquid-liquid interfacial synthesis of ZnBHT	31
2.7.2. Liquid-liquid interfacial synthesis of ZnBHT-H	32
2.7.3. Liquid-liquid interfacial synthesis using different Zn (II) salt	32
2.8. References	34

Chapter 3 Bisdithiolatoiron(II) Coordination Nanosheets

3.1. Introduction	
3.1.1. Rationale of research	35
3.2. Liquid-liquid interfacial synthesis of FeBHT-H (1-H)	36
3.3 Characterization of 1-H	
3.3.1. Transmission Electron Microscopy	36
3.3.2. Scanning Electron Microscopy	37
3.3.3. X-ray Photoelectron Spectroscopy	37
3.3.4. Infrared Spectroscopy	38
3.3.5. UV-visible Spectroscopy	38
3.4. Powder X-Ray Diffraction Studies and Simulations	39
3.5. Electrical Conductivity Measurements	42
3.6. Conclusion	44
3.7. Experimental	44
3.7.1. Liquid-liquid Interfacial Syntheses	45
3.7.2. Temperature-dependent Electrical Conductivity Measurements	45
3.8. References	46

Chapter 4 Fabrication and Transmetallation of Thin Zinc (II) Dithiolene Nanosheets

4.1. Introduction	47
4.1.1. Rationale of Method	48
4.2. Fabrication of large area, thin ZnBHT nanosheets	48
4.3. Transmetallation of ZnBHT nanosheets	49
4.4. Characterization of Transmetallated Dithiolene Nanosheets (tmMDTs)	

4.4.1. Transmetallated Ni (II) Dithiolene Nanosheet (tmNiDT)	
4.4.1.1. Optical Microscopy	50
4.4.1.2. X-Ray Photoelectron Spectroscopy	51
4.4.2. Transmetallated Cu (II) Dithiolene Nanosheet (tmCuDT)	
4.4.2.1. Optical Microscopy	52
4.4.2.2. X-Ray Photoelectron Spectroscopy	52
4.4.3. Transmetallated Fe (II) Dithiolene Nanosheet (tmFeDT)	
4.4.3.1. Optical Microscopy	54
4.4.3.2. X-Ray Photoelectron Spectroscopy	55
4.5. Electrical Conductivity of Transmetallated Metalladithiolene Nanosheet (tmMDTs)	56
4.6. Scanning Electrochemical Cell Microscopy (SECCM) Studies	
4.6.1. Hydrogen Evolution Ability of tmMDTs by SECCM measurement	58
4.6.2. Spatial imaging of tmFeDT-ZnBHT junction	59
4.7. Conclusion	60
4.8. Experimental	60
4.8.1. Synthesis of thin film ZnBHT	61
4.8.2. Area-specific transmetallation of ZnBHT – General Procedure	61
4.9. References	62

Chapter 5 Lateral Heterojunctions by Transmetallation of Zinc (II) Dithiolene Nanosheets

5.1. Introduction	
5.1.1. Vertical Heterostructures of 2D materials	63
5.1.2. Lateral Heterostructures of 2D materials	64
5.1.3. Purpose of Project and Rationale	65
5.2. Fabrication and Characterization of Heterojunctions	66
5.3. Electrical Properties of Heterojunctions	
5.3.1. Measurements of I-V curves of Heterojunctions - Method	68
5.3.2. tmCuDT-tmFeDT Lateral Heterojunction	
5.3.2.1. I-V curve measurements	68
5.3.2.2. Kelvin Probe Force Microscopy (KFM)	70
5.3.3. tmFeDT-tmNiDT Lateral Heterojunction	72

5.3.4. tmNiDT-tmCuDT Lateral Heterojunction	72
5.4. Scanning Electron Microscopy of tmFeDT-tmCuDT Lateral Heterojunction	73
5.5. Possible mechanisms of rectification	
5.5.1. As a p-n junction	72
5.5.2. As a p^+ -p junction	73
5.5.3. As a metal-semiconductor junction	73
5.6. Conclusion	74
5.7. Experimental	
5.7.1. Transmetallation of tmCuDT/ZnBHT to form tmCuDT/tmFeDT heterojunction	
5.7.2. Transmetallation of tmCuDT/ZnBHT to form tmCuDT/tmNiDT heterojunction	
5.7.3. Transmetallation of tmNiDT/ZnBHT to form tmNiDT/tmFeDT heterojunction	75
5.8. References	76
 Chapter 6 Conclusion	
6.1. Conclusion and Perspective	78
6.2. References	79
 Acknowledgements	80
 List of Publications	82

Chapter 1

General Introduction

1.1. Introduction: 2-Dimensional Materials

As the quest for developing smaller devices continues, the dive into nanomaterials is intensifying. In the process, scientists look toward to creating materials with dimensionality that is tailor-made to their preferences. Materials with zero dimensionality such as metal complexes and quantum dots for example, enable scientists to develop devices such as LEDs. Moving into one-dimensional materials, nanowires have shown various properties such as high conductivity and fluorescence. Three-dimensional (3D) materials compose a huge part of daily life, from biological molecules to porous zeolites and artificial polymeric materials.

2D structures in the form of nanosheets, are the focus of this thesis. 2D materials are widely researched in the current scientific field, as the ability to develop create large area, thin (or mono layer) frameworks allows us to access varying areas such as catalysis, semiconductivity, electrochromism or photoresponsiveness. In addition, the physical properties of monolayer thin films also give rise to unusual physical properties such as topological insulator states¹, which can be very different from their layered 3D counterparts. The paradigm of 2-dimensional materials is graphene.

1.1.1. Graphene

The isolation of single layer graphene – which had existed for many years but under the guise of its 3-dimensional form graphite – by Geim and Novoselov² in 2004 led to the ‘graphene gold rush’ – a frenzy of research activity on the properties of graphene and its various applications, which continues until today. Since then, novel physical properties and phenomena continue to be observed in graphene, such as the quantum Hall effect at room temperature³ and the Dirac fermion nature of its electrons⁴. Furthermore, the use of graphene in heterostructures layered with other materials such as BN or MoS₂ has led to the discovery of new phenomena such as field effect tunneling⁵ and photothermionic effects⁶. Graphene heterostructure devices, such as h-BN-graphene structures⁷, also overcome the lack of a band gap at the Dirac point of graphene, while maintaining the high carrier mobility that graphene offers, making them good candidates for integrated circuits.

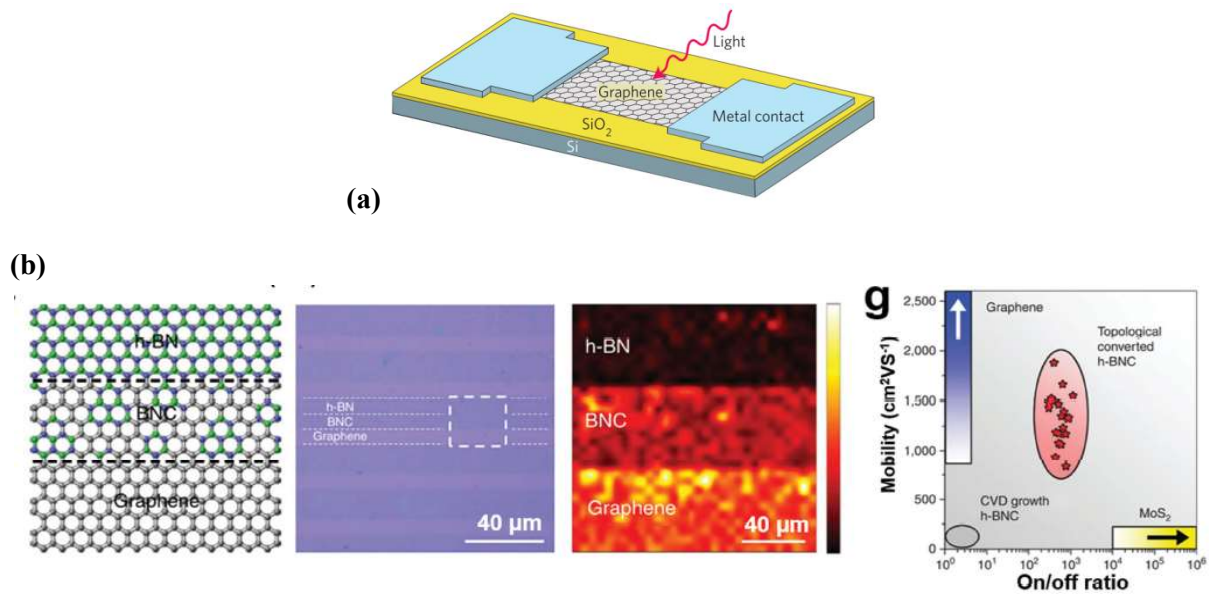


Figure 1-1. a) A graphene photodetector⁸; b) Hetero-BN-graphene heterostructure with high mobility and good on-off ratio⁹. Reproduced with permission from Springer Nature (ref. 8) and John Wiley & Sons (ref. 9).

Having opened the door to the world of 2-dimensional materials, intense research efforts inspired by the discovery of graphene has led to many discoveries in the field of condensed matter physics, resulting in the discovery and advancements of technologies involving 2D materials. Research has now expanded to involve many different types of layered materials.

1.1.2. Layered Double Hydroxides

Layered double hydroxides (LDHs) exhibit an unusual property compared to typical metal hydroxides: LDHs have positively charged layers (vs. negatively charged layers in typical metal hydroxides) with exchangeable anions in the interlayer. With the general formula of $M^{II}_{1-x}M^{III}_x(OH)_2(A^{n-})_{x/n} \cdot mH_2O$ ¹⁰, LDHs typically consist of a combination of divalent and trivalent metal ions, which are sought after as catalysts due to their diversity and stability.¹¹ The ease of exchange of the intercalated anions also provides unique methods of exfoliating single layer nanosheets. In particular, by interchanging a small intercalated ion (e.g. Br^-) with a larger one (e.g. NO_3^- or CO_3^{2-}), the interlayer spacing is increased, with corresponding weakening of interlayer attraction. Dispersion after stirring in solution leads to monolayers being formed.¹² Examples of applications involving LDHs are spintronics¹³, electrodes in pseudocapacitors¹⁴ and also for the removal of heavy metals¹⁵.

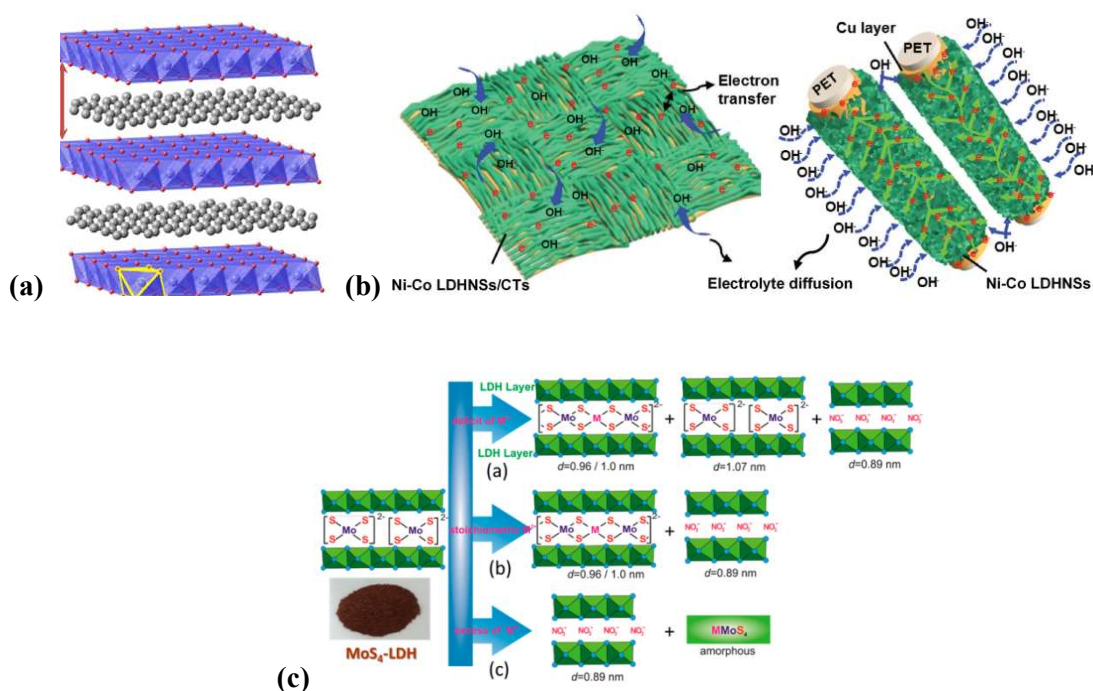


Figure 1-2. (a) A typical LDH showing layers (blue) and intercalated anions (grey)¹¹; (b) LDHs deposited on conductive textile (CT) for use as pseudocapacitors¹⁴ and (c) removal of heavy metals by precipitation with intercalated MoS_4^- anions in an LDH.¹⁵ Reproduced with permission from AAAS (ref. 11), the Royal Society of Chemistry (ref. 14) and the American Chemical Society (ref. 15).

1.1.3. Transition Metal Dichalcogenides (TMDs)

TMDs are semiconductors with the formula MX_2 , M being a transition metal (Mo, W etc.) and X being a chalcogen (S, Se or Te). Monolayers of TMDs exhibit various useful properties such as having a direct band gap¹⁶, strong spin orbit coupling leading to spin control¹⁷ and the lack of an inversion center in the monolayer crystal structure opens up a new field known as valleytronics¹⁸. Improvements in the synthetic methods of TMDs and nanomaterials by techniques such as chemical vapor deposition¹⁹ or bottom up synthetic methods²⁰ have widened the applications of TMDs. Some of these applications include MoS_2 monolayer FET devices with excellent ON/OFF ratios²¹, electrocatalytic hydrogen production²², and large area, transparent and flexible electronics.²³

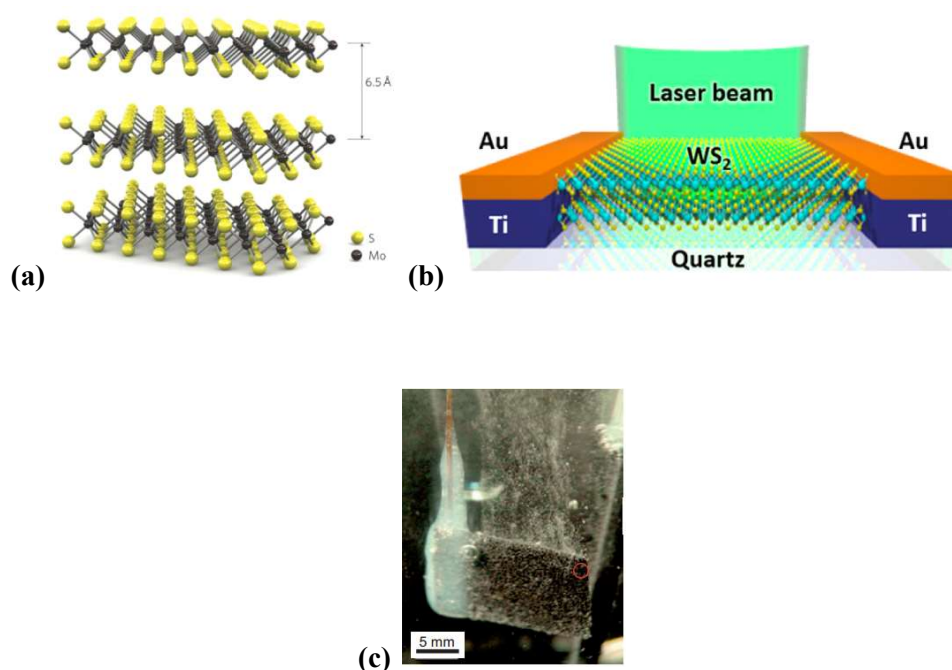


Figure 1-3. (a) Structure of a typical layered TMD²⁴; (b) Schematic of a photoelectric device utilizing few layer WS_2 ²⁴; (c) Graphene-protected Ni foam on which MoS_2 films were grown, being used in hydrogen evolution reaction²². Reproduced with permission from the American Chemical Society (refs. 22 and 24).

1.1.4. Surface Covalent-Organic Frameworks (*surCOFs*)

SurCOFs are crystalline extended organic structures whereby the fundamental units are covalently bonded, and the structures are grown on a substrate surface. The surfaces can act as templates that facilitate the ordered coordination and subsequent bonding to take place, such as graphene which has pores aligned in the same direction.²⁵ The covalent framework imparts robustness to the entire framework and depending on the functional groups of the building blocks used, provides a stable and modular platform for various applications. For example, fluorescent dyes and hydrophilic polymers could be attached for gas separations or catalysis²⁶, or the intrinsic properties of the building blocks impart photo-responsiveness to the sheet.²⁷ The use of ordered metal substrates can promote both the ordered coordination of building blocks and bond-formation between the blocks, allowing COF synthesis under UHV²⁸.

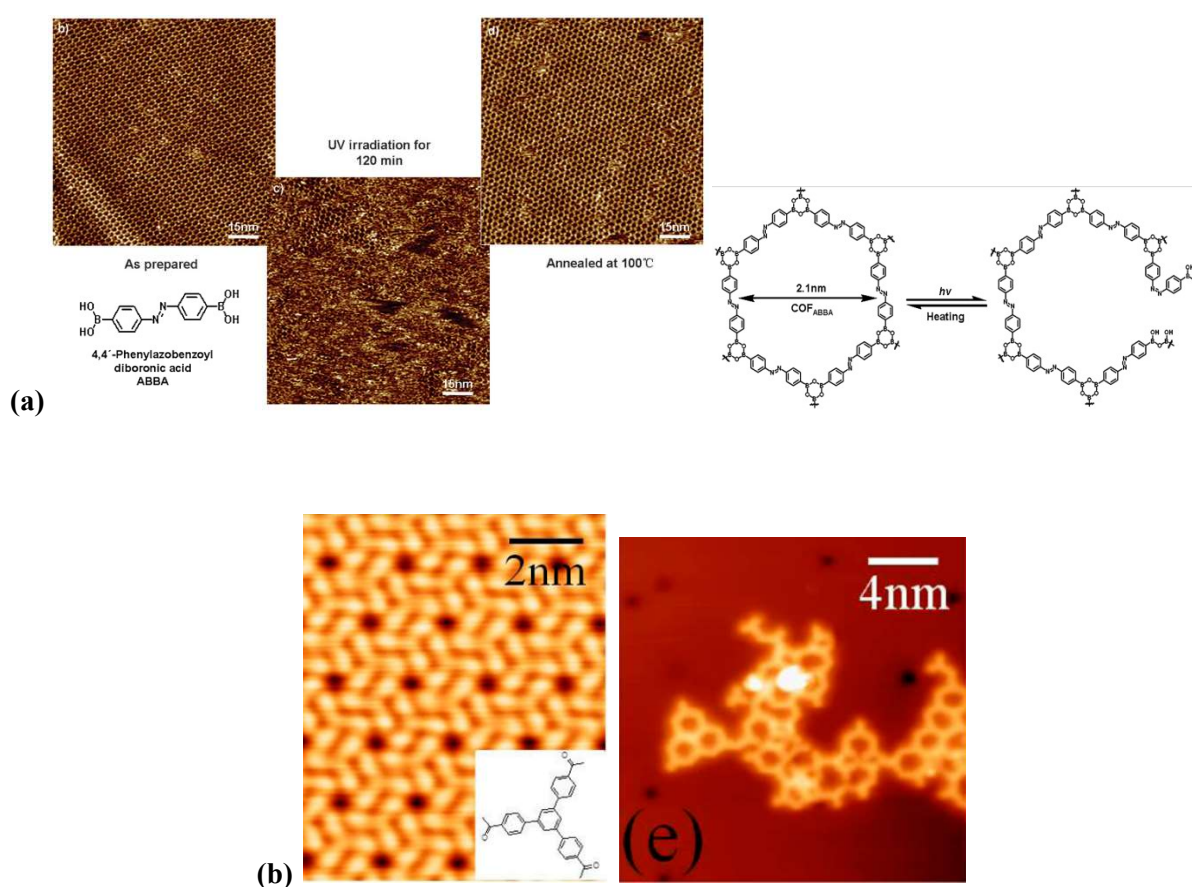


Figure 1-4. (a) Photoresponsive *surCOF* synthesized with 4,4'-Phenylazobenzoyl diboronic acid (ABBA) building blocks, showing disruption of ordered structure after UV irradiation²⁷; (b) Synthesis of *surCOF* with 1,3,5-tris(4-acetylphenyl)benzene (TAPB): Left: STM image after room temperature deposition, Right: STM image after substrate heated to 590K.²⁸ Reproduced with permission from John Wiley & Sons (ref. 27) and the American Chemical Society (ref. 28).

1.1.5. Metal-Organic Coordination Nanosheets (CONASHs)

Metal-organic coordination networks, commonly called coordination nanosheets, consist of metal ions coordinated to ligands in an extended framework, as the name suggests. Furthermore, our group has suggested the term CONASH, an abbreviation of **CO**ordination **NA**no**SH**eets, to refer to this class of materials. Many such types of CONASHs have been reported.^{29–31} The biggest advantage of these CONASHs is modularity: CONASHs with a wide spectrum of physical properties can be obtained by simply changing either the metal ion or ligand used. There are multiple reports about CONASHs showing redox tunability³², electrochromism³³, photofunctionality³⁴, high conductivity^{35,36}, catalysts in hydrogen production^{37,38} and also chemical sensing³⁹. As scientists design ever more unique molecules with novel properties, it is expected that CONASHs will unlock the door to an enormous array of new materials.

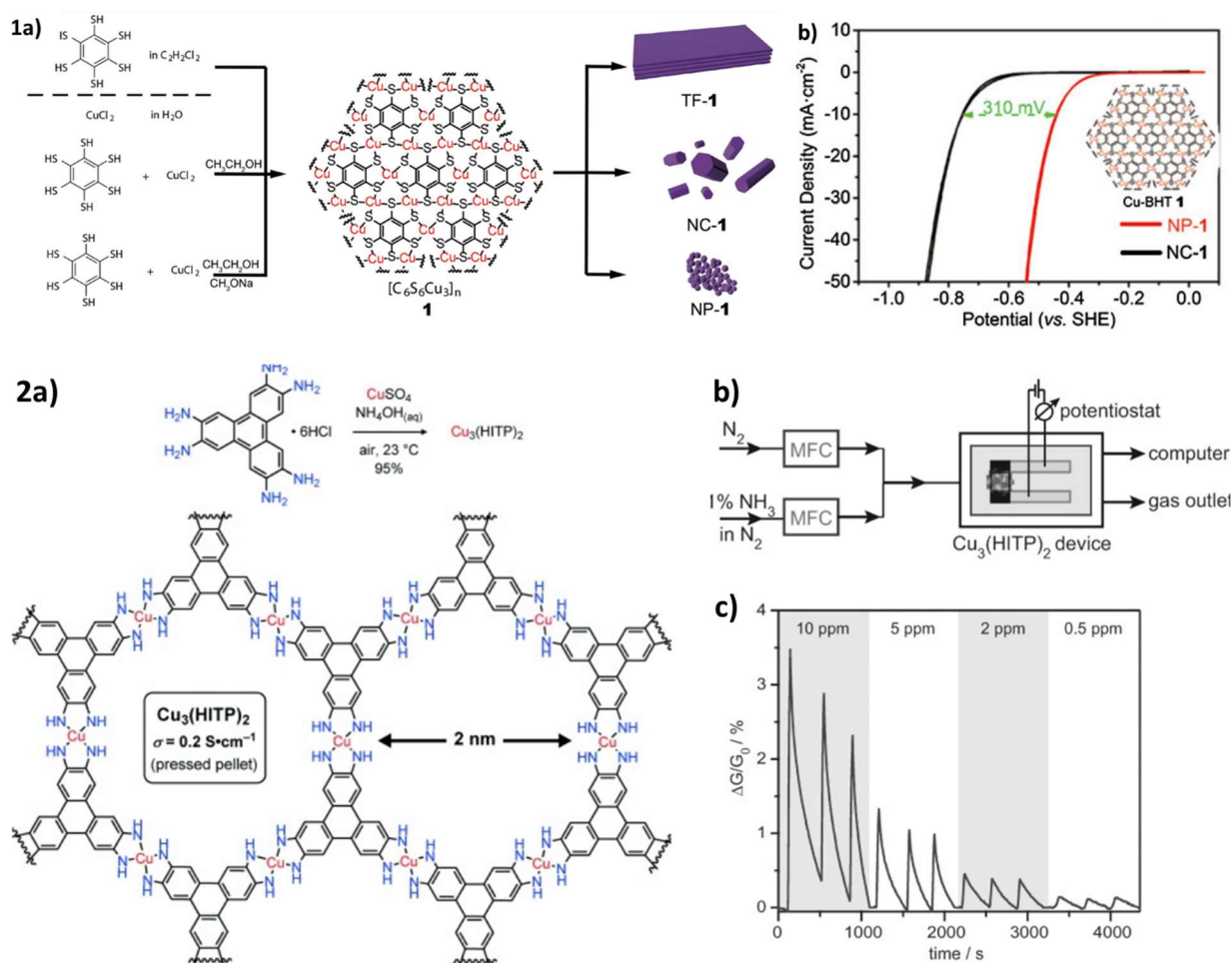


Figure 1-5. (1a) Three methods of synthesizing copper-benzenehexathiol (Cu-BHT) coordination materials and their morphologies, (1b) Hydrogen-evolution catalysis studies of nanoparticle (NP) and nanocrystal (NC) Cu-BHT materials³⁸; (2a) Synthetic scheme of Cu₃(HITP)₂ material, (2b) Chemical sensing experimental setup of Cu₃(HITP)₂, (2c) Relative responses of Cu₃(HITP)₂ material to varying concentrations of NH₃ gas in N₂.³⁹ Reproduced with permission from the American Chemical Society (ref. 38) and John Wiley & Sons (ref. 39).

1.2. Fabricating nanosheets – Approaches

1.2.1. Top-down approach

Nanosheets may be fabricated by either of two methods: top down or bottom up. In the top down approach, nanosheets are obtained from the bulk 3-dimensional source material by methods such as exfoliation from layered materials^{40,41}, (e.g. the micromechanical exfoliation ('Scotch tape') method that famously led to the isolation of single layer graphene⁴², or ion-intercalation followed by agitation to cause layer separation.⁴³

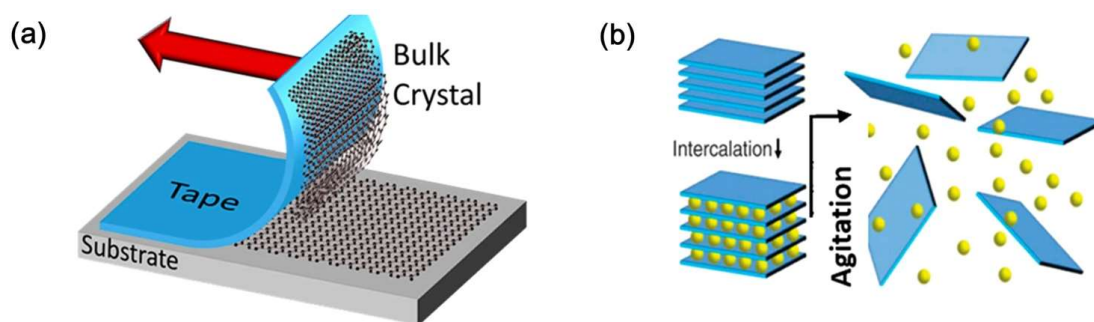


Figure 1-6. Top-down nanosheet formation by micromechanical exfoliation using sticky tape (left); intercalation and agitation-dispersion method (right).⁴³ Reproduced with permission from Creative Commons.

In the context of coordination nanosheets, these methods have inherent disadvantages. During the synthesis of bulk materials, it is difficult to control the structure of the resulting material such as thickness or domain sizes. Mechanical methods such as sonication or micromechanical exfoliation can cause massive structural disruption, leading to the breaking of metal-ligand bonds and hence reducing the domain size of nanosheets produced. Hence an alternative method must be developed to produce nanosheets with large area and yet can be isolated with few layer thicknesses.

1.2.2. Bottom-up approach

In the bottom-up approach, nanosheets are formed from its component parts (e.g. metal ion and ligand) which are combined in a controlled manner. Not only is this process amenable by changing the metal or ligand, it also allows the synthesis of thin or even monolayer nanosheets with large areas, by processes such as chemical vapour deposition.

The method commonly used in the study of dithiolene CONASHs is the liquid-liquid interfacial method. The interface where two immiscible liquids meet provides a flat, 2-dimensional area whereby reactions can take place. Together with systems that can inherently form planar structures (e.g. d^8 metals such as Ni^{2+} with aryl ligands such as BHT) this method allows the formation of large domain nanosheets.³⁴

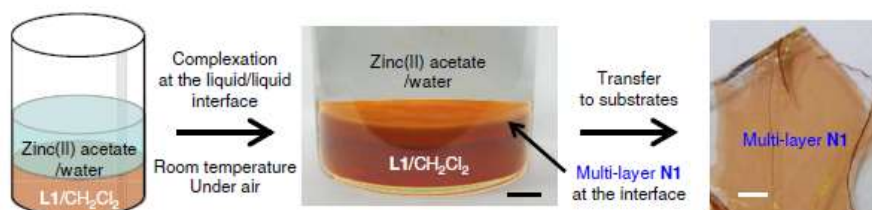


Figure 1-7. Liquid-liquid interfacial reaction producing large area zinc-bis(dipyrinato) (N1) nanosheet.³⁴ Reproduced with permission from Springer Nature.

1.3. Dithiolene Chemistry

Dithiolenes are a group of sulfur-based ligands that bind to metal ions through 2 thiolate groups located on adjacent carbons, usually conjugated with a double bond or π -system. The π -conjugated system causes the unusual binding modes of dithiolenes, binding to the metal ion in a typical thiolate fashion (where the S atom has a formal oxidation state of -1), or in a thione fashion (where the S atom has a formal oxidation state of 0).⁴⁴ This causes the coordinated ligand to be redox-flexible and is often the source of redox activity in these nanosheets.⁴⁵ It also results in the central metal atom adopting different formal oxidation states. Although many previous studies had been conducted on bisdithiolene complexes, there had been no reports of extended CONASHs made with bisdithiolene complexes until the pioneering work of Kambe et. al.⁴⁶

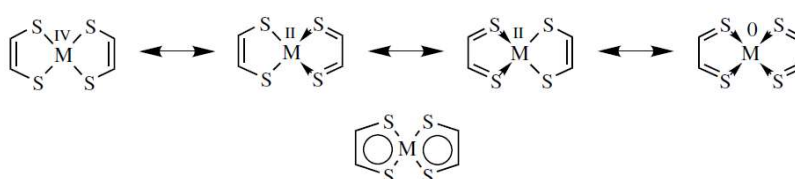


Figure 1-8. Multiple binding modes of bis-dithiolene complexes leading to different formal oxidation states of the central metal ion.⁴⁴ Reproduced with permission from John Wiley & Sons.

1.4. CONASHs using Benzenhexathiol (BHT) ligand

The use of Ni (II) ion, a d^8 metal ion which typically forms square planar complexes, together with the planar benzenhexathiol (BHT) ligand, successfully gave the NiBHT nanosheet which was subsequently characterized to be redox tunable and highly conductive.^{46,47} Other reports have extended the BHT nanosheet system to include other metal ions: PdBHT nanosheets are electrically conductive⁴⁸, PtBHT nanosheets are potential room temperature topological insulators⁴⁹, CuBHT nanosheets exhibit superconductivity⁵⁰ and ambipolar charge transport⁵¹. CoBHT nanosheets proved to be an efficient catalyst in the hydrogen evolution reaction⁵², while AgBHT⁵³ and Cu(I)BHT⁵⁴ form in rare 3-dimensional structures with high conductivity. In situ one-pot synthesis strategy was also employed to access the Au(III)BHT, which was prone to unwanted reduction to form Au nanoparticles.⁵⁵ These examples only serve to show the wide range of physical phenomena possible by simply changing the metal ion in the BHT system.

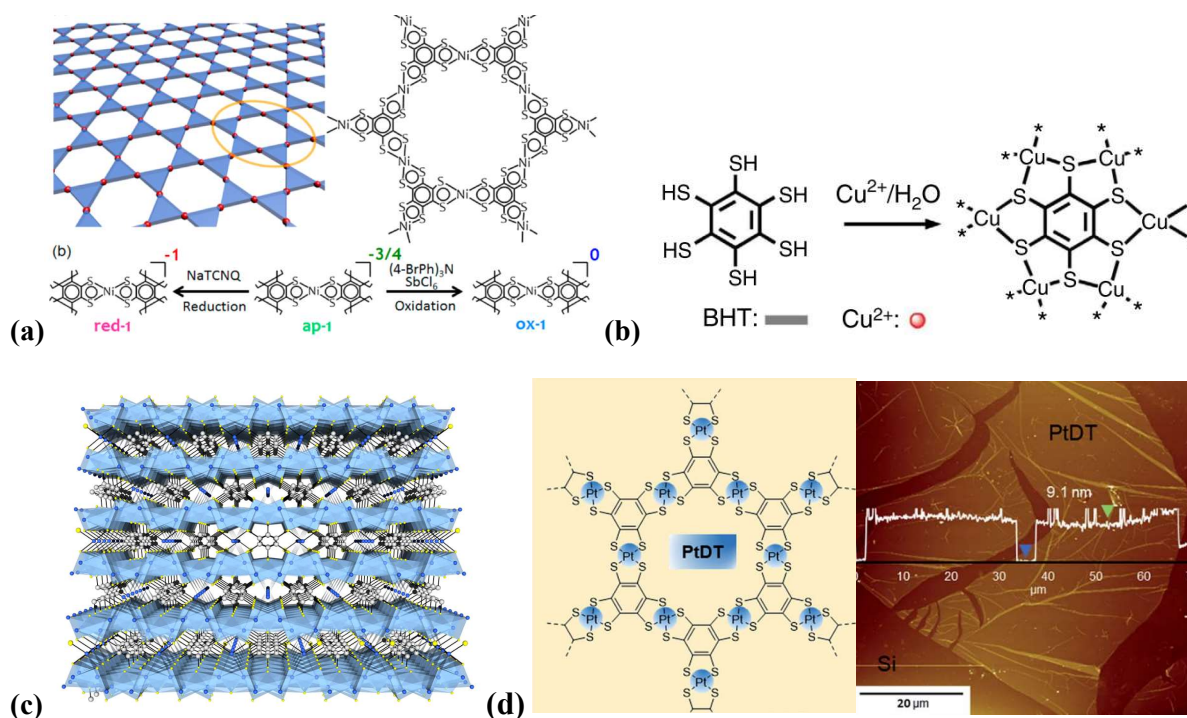


Figure 1-9. (a) NiBHT exhibiting variable oxidation states⁴⁷; (b) Chemical structure of CuBHT⁵¹; (c) 3D network of AgBHT⁵³; (d) Chemical structure and AFM image of PtDT nanosheet.⁴⁹ Reproduced with permission from the American Chemical Society (refs. 47,53), Springer Nature (ref. 51) and the Royal Society of Chemistry (ref. 49).

1.5. Thesis Outline

Novel metal-organic CONASHs can be produced by varying either the ligand or metal. Previous examples outlined in the introduction section considered the wide range of ligands used to produce functional CONASHs. On the other hand, there is still much to be explored about the BHT system, such as what happens if the metal ion is changed while using a pre-existing ligand, or what new physical properties might arise through the combination of these materials in hybrid systems. Hence, this thesis will explore these two main directions, revolving around the common ligand benzenhexathiol.

Including the introduction chapter, this thesis is divided into 6 chapters: Chapter 2 describes the synthesis of zinc (II) dithiolene CONASH, Chapter 3 highlights my efforts to synthesize and elucidate the structure of iron (II) dithiolene nanosheets. Chapter 4 details the transmetallation of zinc (II) dithiolene nanosheets while Chapter 5 explores the physical properties of lateral heterojunctions produced by transmetallation. Chapter 6 summarizes the significant results of my study and outlines some thoughts for future research.

1.6. References

- (1) Wang, Z.; Su, N.; Liu, F. T. *Nano Lett.* **2013**, *13*, 2842.
- (2) Novoselov, K. S.; Geim, A. K.; Morozov, S. V.; Jiang, D.; Zhang, Y.; Dubonos, S. V.; Grigorieva, I. V; Firsov, A. A. *Science* **2004**, *306*, 666.
- (3) Novoselov, K. S.; Geim, A. K.; Morozov, S. V.; Jiang, D.; Katsnelson, M. I.; Grigorieva, I. V; Dubonos, S. V; Firsov, A. A. *Nature* **2005**, *438*, 197.
- (4) Geim, A. K.; Novoselov, K. S. *Nat. Mater.* **2007**, *6*, 183.
- (5) Britnell, L.; Gorbachev, R. V.; Jalil, R.; Belle, B. D.; Schedin, F.; Mishchenko, A.; Georgiou, T.; Katsnelson, M. I.; Eaves, L.; Morozov, S. V.; Peres, N. M. R.; Leist, J.; Geim, A. K.; Novoselov, K. S.; Ponomarenko, L. A. *Science* **2012**, *335*, 947.
- (6) Massicotte, M.; Schmidt, P.; Vialla, F.; Watanabe, K.; Taniguchi, T.; Tielrooij, K. J.; Koppens, F. H. L. *Nat. Commun.* **2016**, *7*, 1.
- (7) Fiori, G.; Bonaccorso, F.; Iannaccone, G.; Palacios, T.; Neumaier, D.; Seabaugh, A.; Banerjee, S. K.; Colombo, L. *Nat. Nanotechnol.* **2014**, *9*, 768.
- (8) Bonaccorso, F.; Sun, Z.; Hasan, T.; Ferrari, A. C. *Nat. Photonics* **2010**, *4*, 611.
- (9) Li, Q.; Liu, M.; Zhang, Y.; Liu, Z. *Small* **2016**, *12*, 32.
- (10) Liu, Z.; Ma, R.; Ebina, Y.; Iyi, N.; Takada, K.; Sasaki, T. *Langmuir* **2007**, *23*, 861.
- (11) Suntivich, J.; May, K. J.; Gasteiger, H. A.; Goodenough, J. B.; Shao-Horn, Y. *Science* **2011**, *334*, 1383.

- (12) Song, F.; Hu, X. *Nat. Commun.* **2014**, 5, 1.
- (13) Coronado, E.; Mart, C.; Waerenborgh, J.; Ribera, A. **2013**.
- (14) Nagaraju, G.; Raju, G. S. R.; Ko, Y. H.; Yu, J. S. *Nanoscale* **2015**, 8, 812.
- (15) Ma, L.; Wang, Q.; Islam, S. M.; Liu, Y.; Ma, S.; Kanatzidis, M. G. *J. Am. Chem. Soc.* **2016**, 138, 2858.
- (16) Ross, J. S.; Klement, P.; Jones, A. M.; Ghimire, N. J.; Yan, J.; Mandrus, D. G.; Taniguchi, T.; Watanabe, K.; Kitamura, K.; Yao, W.; Cobden, D. H.; Xu, X. *Nat. Nanotechnol.* **2014**, 9, 268.
- (17) Reyes-Retana, J. A.; Cervantes-Sodi, F. *Sci. Rep.* **2016**, 6, 24093.
- (18) Zeng, H.; Dai, J.; Yao, W.; Xiao, D.; Cui, X. *Nat. Nanotechnol.* **2012**, 7, 490.
- (19) Chhowalla, M.; Shin, H. S.; Eda, G.; Li, L.-J.; Loh, K. P.; Zhang, H. *Nat. Chem.* **2013**, 5, 263.
- (20) Zhao, M.; Wang, Y.; Ma, Q.; Huang, Y.; Zhang, X.; Ping, J.; Zhang, Z.; Lu, Q.; Yu, Y.; Xu, H.; Zhao, Y.; Zhang, H. *Adv. Mater.* **2015**, 27, 7372.
- (21) Radisavljevic, B.; Whitwick, M. B.; Kis, A. *ACS Nano* **2011**, 5, 9934.
- (22) Chang, Y. H.; Lin, C. Te; Chen, T. Y.; Hsu, C. L.; Lee, Y. H.; Zhang, W.; Wei, K. H.; Li, L. J. *Adv. Mater.* **2013**, 25, 756.
- (23) Pu, J.; Yomogida, Y.; Liu, K. K.; Li, L. J.; Iwasa, Y.; Takenobu, T. *Nano Lett.* **2012**, 12, 4013.
- (24) Lv, R.; Robinson, J. A.; Schaak, R. E.; Sun, D.; Sun, Y.; Mallouk, T. E.; Terrones, M. *Acc. Chem. Res.* **2015**, 48, 56.
- (25) Dogru, M.; Bein, T. *Nat. Nanotechnol.* **2011**, 6, 333.
- (26) Calik, M.; Sick, T.; Dogru, M.; Döblinger, M.; Datz, S.; Budde, H.; Hartschuh, A.; Auras, F.; Bein, T. *J. Am. Chem. Soc.* **2016**, 138, 1234.
- (27) Liu, C.; Zhang, W.; Zeng, Q.; Lei, S. *Chem. Eur. J.* **2016**, 22, 6768.
- (28) Yang, B.; Björk, J.; Lin, H.; Zhang, X.; Zhang, H.; Li, Y.; Fan, J.; Li, Q.; Chi, L. *J. Am. Chem. Soc.* **2015**, 137, 4904.
- (29) Makiura, R.; Konovalov, O. *Sci. Rep.* **2013**, 3, Article 2506.
- (30) Makiura, R.; Motoyama, S.; Umemura, Y.; Yamanaka, H.; Sakata, O.; Kitagawa, H. *Nat. Mater.* **2010**, 9, 565.
- (31) Liu, K.; Wang, L.; Dong, R. *J. Mater. Chem. C* **2020**, 8, 10696.

- (32) Kambe, T.; Sakamoto, R.; Kusamoto, T.; Pal, T.; Fukui, N.; Hoshiko, K.; Shimojima, T.; Wang, Z.; Hirahara, T.; Ishizaka, K.; Hasegawa, S.; Liu, F.; Nishihara, H. *J. Am. Chem. Soc.* **2014**, *136*, 14357.
- (33) Takada, K.; Sakamoto, R.; Yi, S. T.; Katagiri, S.; Kambe, T.; Nishihara, H. *J. Am. Chem. Soc.* **2015**, *137*, 4681.
- (34) Sakamoto, R.; Hoshiko, K.; Liu, Q.; Yagi, T.; Nagayama, T.; Kusaka, S.; Tsuchiya, M.; Kitagawa, Y.; Wong, W.-Y.; Nishihara, H. *Nat. Commun.* **2015**, *6*, 6713.
- (35) Sheberla, D.; Sun, L.; Blood-Forsythe, M. a; Er, S.; Wade, C. R.; Brozek, C. K.; Aspuru-Guzik, A.; Dincă, M. *J. Am. Chem. Soc.* **2014**, *136*, 8859.
- (36) Melot, B. C.; Clough, A. J.; Marinescu, S. C.; Downes, C. A.; Walsh, A.; de la Rosa, A. A.; Yoo, J. W.; Skelton, J. M. *J. Am. Chem. Soc.* **2017**, *139*, 10863.
- (37) Clough, A. J.; Yoo, J. W.; Mecklenburg, M. H.; Marinescu, S. C. *J. Am. Chem. Soc.* **2015**, *137*, 118.
- (38) Huang, X.; Yao, H.; Cui, Y.; Hao, W.; Zhu, J.; Xu, W.; Zhu, D. *ACS Appl. Mater. Interfaces* **2017**, *9*, 40752.
- (39) Campbell, M. G.; Sheberla, D.; Liu, S. F.; Swager, T. M.; Dinca, M. *Angew. Chemie - Int. Ed.* **2015**, *54*, 4349.
- (40) Zhao, W.; Xue, Z.; Wang, J.; Jiang, J.; Zhao, X.; Mu, T. *ACS Appl. Mater. Interfaces* **2015**, *7*, 27608.
- (41) Coleman, J. N.; Lotya, M.; O'Neill, A.; Bergin, S. D.; King, P. J.; Khan, U.; Young, K.; Gaucher, A.; De, S.; Smith, R. J.; Shvets, I. V.; Arora, S. K.; Stanton, G.; Kim, H.-Y.; Lee, K.; Kim, G. T.; Duesberg, G. S.; Hallam, T.; Boland, J. J.; Wang, J. J.; Donegan, J. F.; Grunlan, J. C.; Moriarty, G.; Shmeliov, A.; Nicholls, R. J.; Perkins, J. M.; Grieveson, E. M.; Theuwissen, K.; McComb, D. W.; Nellist, P. D.; Nicolosi, V. *Science* **2011**, *331*, 568.
- (42) Novoselov, K. S.; Jiang, D.; Schedin, F.; Booth, T. J.; Khotkevich, V. V.; Morozov, S. V.; Geim, A. K. *Proc. Natl. Acad. Sci. U. S. A.* **2005**, *102*, 10451.
- (43) Sekhon, S. S.; Kaur, P.; Kim, Y. H.; Sekhon, S. S. *npj 2D Mater. Appl.* **2021**, *5*, 1.
- (44) Beswick, C.L.; Schulman, J.M.; Stiefel, E. I. Structures and Structural Trends in Homoleptic Dithiolene Complexes. In *Dithiolene Chemistry: Progress in Inorganic Chemistry*; John Wiley & Sons: Hoboken, New Jersey, 2003; pp 57–58.
- (45) Kusamoto, T.; Nishihara, H. *Coord. Chem. Rev.* **2019**, *380*, 419.
- (46) Kambe, T.; Sakamoto, R.; Hoshiko, K.; Takada, K.; Miyachi, M.; Ryu, J.; Sasaki, S.; Kim, J.; Nakazato, K.; Takata, M.; Nishihara, H. *J. Am. Chem. Soc.* **2013**, *135*, 2462.

- (47) Kambe, T.; Sakamoto, R.; Kusamoto, T.; Pal, T.; Fukui, N.; Hoshiko, K.; Shimojima, T.; Wang, Z.; Hirahara, T.; Ishizaka, K.; Hasegawa, S.; Liu, F.; Nishihara, H. *J. Am. Chem. Soc.* **2014**, *136*, 14357.
- (48) Pal, T.; Kambe, T.; Kusamoto, T.; Foo, M. L.; Matsuoka, R.; Sakamoto, R.; Nishihara, H. *ChemPlusChem* **2015**, *80*, 1255.
- (49) Pal, T.; Doi, S.; Maeda, H.; Wada, K.; Tan, C. M.; Fukui, N.; Sakamoto, R.; Tsuneyuki, S.; Sasaki, S.; Nishihara, H.; Meng, C.; Fukui, N. *Chem. Sci.* **2019**, *10*, 5218.
- (50) Huang, X.; Zhang, S.; Liu, L.; Yu, L.; Chen, G.; Xu, W.; Zhu, D. *Angew. Chem. Int. Ed.* **2018**, *57*, 146.
- (51) Huang, X.; Sheng, P.; Tu, Z.; Zhang, F.; Wang, J.; Geng, H.; Zou, Y.; Di, C.; Yi, Y.; Sun, Y.; Xu, W.; Zhu, D. *Nat. Commun.* **2015**, *6*, 7408.
- (52) Downes, C. A.; Clough, A. J.; Chen, K.; Yoo, J. W.; Marinescu, S. C. *ACS Appl. Mater. Interfaces* **2018**, *10*, 1719.
- (53) Huang, X.; Li, H.; Tu, Z.; Liu, L.; Wu, X.; Chen, J.; Liang, Y.; Zou, Y.; Yi, Y.; Sun, J.; Xu, W.; Zhu, D. *J. Am. Chem. Soc.* **2018**, *100190*, 15153.
- (54) Huang, X.; Qiu, Y.; Wang, Y.; Liu, L.; Wu, X.; Liang, Y.; Cui, Y.; Sun, Y.; Zou, Y.; Zhu, J.; Fang, W.; Sun, J.; Xu, W.; Zhu, D. *Angew. Chemie - Int. Ed.* **2020**, *59*, 22602.
- (55) Chen, I. F.; Lu, C. F.; Su, W. F. *Langmuir* **2018**, *34*, 15754.

Chapter 2

Bisdithiolatozinc (II) Coordination Nanosheets

本章については、5 年以内雑誌等で刊行予定のため、非公開。

Chapter 3

Bisdithiolatoiron(II) Coordination Nanosheets

3.1. Introduction

Iron is one of the major elements in the earth and possesses a wide variety of interesting chemical and physical properties, the reason why iron coordination materials have been extensively studied. From redox activity and conductivity to ferromagnetism, the combination of iron with organic molecules greatly expands the number of novel materials that can be synthesized and explored.

Recently, the development of dithiolene coordination materials utilizing Fe (II) has picked up pace. A framework based on iron (II) coordination with perthiolated coronene exhibits good electrical conductivity and ferromagnetism.¹ Hall effect measurements and terahertz photoconductivity experiments on another framework which uses triphenylene-hexathiol (THT) to give $\text{Fe}_3(\text{THT})_2(\text{NH}_4)_3$ elucidated its band-like charge transport mechanism.²

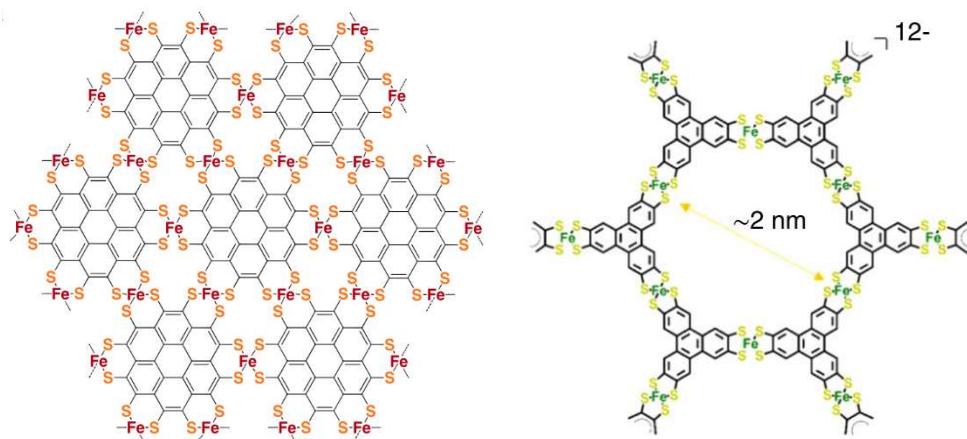


Figure 3-1. Chemical structures of iron (II) dithiolene coordination frameworks using perthiolated coronene¹ (left) and using triphenylene-hexathiol² (right). Reproduced with permission from Creative Commons (ref. 1), and Springer Nature (ref. 2).

3.1.1. Rationale of research

For the BHT system, iron (II) has been utilized in a previously reported study to fabricate Fe-BHT coordination nanosheet.³ It was compared with other metalladithiolene nanosheet analogues, Ni-BHT and Co-BHT and their hydrogen evolution abilities evaluated. Despite the synthesis of the novel Fe-BHT, the authors did not further characterize the material, possibly due to its poor performance in the hydrogen evolution reaction study. However, it is meaningful to both determine the chemical structure of FeBHT and find methods to improve its physical properties, which would enable further research into this promising material.

3.2. Liquid-liquid interfacial synthesis of FeBHT-H (1-H)

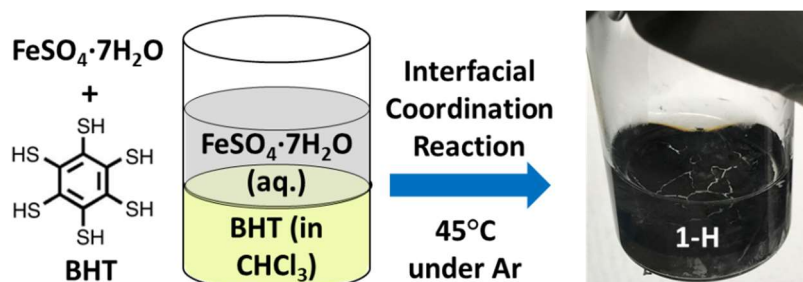


Figure 3-2. Schematic of interfacial synthesis of **1-H**.

In the case of the bisdithiolatozinc(II) nanosheet, it was observed that synthesis under heated condition improved the overall crystallinity of the ZnBHT nanosheet. Because of this, FeBHT-H (abbreviated with **1-H**) was also synthesized with heating at 45 °C. By dissolving BHT in degassed chloroform, layering with water acting as a buffer layer followed by dropwise addition of $\text{FeSO}_4 \cdot 7\text{H}_2\text{O}$ and heating at 45 °C for 24 hours, a lustrous black film was formed at the interface. The film was then washed with water and chloroform, the phases homogenized by addition of ethanol, and **1-H** was either scooped onto substrates for further analysis or filtered and dried under vacuum to obtain a black solid.

3.3. Characterization of 1-H

3.3.1. Transmission Electron Microscopy

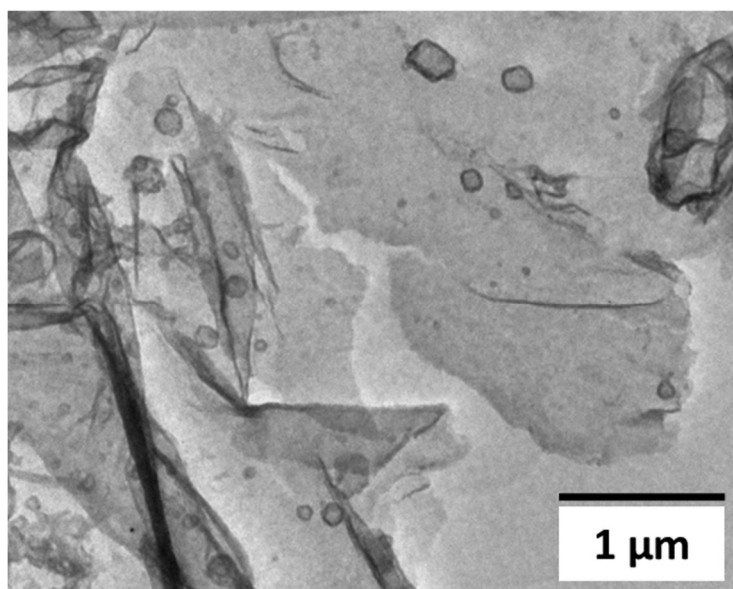


Figure 3-3. HR-TEM image of **1-H** showing sheet-like morphology.

Transmission electron microscopy images of **1-H** reveal its sheet-like morphology (Fig 3-3.). The nanosheets near the left edge of the image show creases and wrinkles caused by random folding of the nanosheet when dropcasted onto the TEM copper grid.

3.3.2 Scanning Electron Microscopy

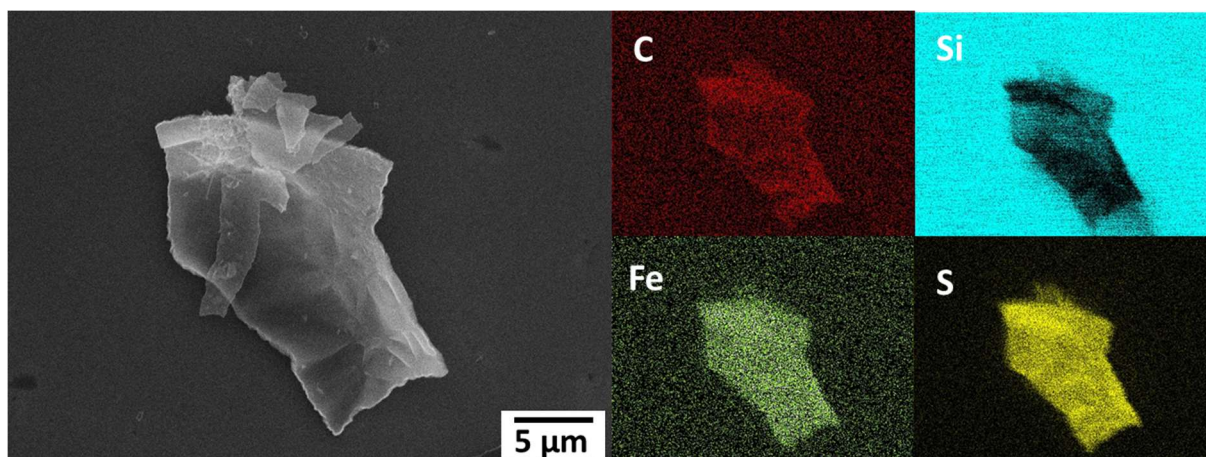


Figure 3-4. SEM image of **1-H** (left); EDS mapping of **1-H** showing presence of elements C, Fe, S in **1-H**.

SEM images taken of **1-H** on Si substrate further show the sheet-like morphology of **1-H**, with multiple flakes layered upon each other (Fig. 3-4). EDS mapping of **1-H** shows the even distribution of elements C, S and Fe in **1-H**, indicating that the nanosheets contain Fe ions coordinated with the BHT ligand.

3.3.3 X-Ray Photoelectron Spectroscopy

XPS measurements of **1-H** give insight to the bonding of the Fe and S atoms within **1-H**. The main Fe2p peaks at 708.6 eV and 721.4 eV in the Fe2p narrow spectrum are attributed to the Fe (II) centers within the nanosheet.

Deconvolution of the S2p spectrum gives 2 pairs of peaks which are assigned to S_{crystal} (163.4 eV and 164.5 eV) followed by S_{defect} (162.2 eV and 163.3 eV) (Fig. 3-5). The small peak at ca. 168 eV is likely due to the residual sulfate ions or small number of oxidized S-O units at the nanosheet domain edges. Quantitative analysis of the Fe and S signals give a Fe:S ratio of 1:2.9. The excess in S content is possibly due to uncoordinated C-S moieties at the domain edges or defects. These results show that coordination between Fe (II) ions and thiol groups of BHT has indeed occurred, giving an extended nanosheet framework.

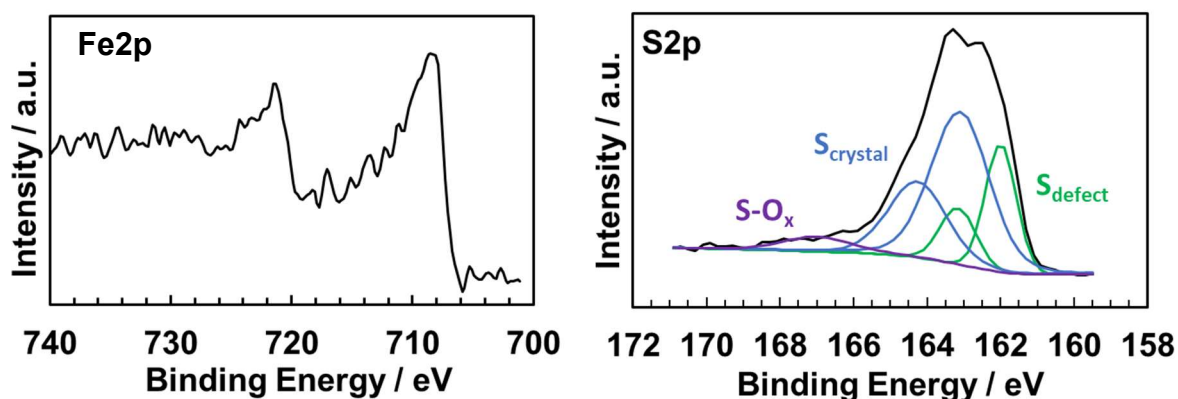


Figure 3-5. XPS narrow spectrum of **1-H**: Fe2p (left) and S2p (right).

3.3.4. Infrared Spectroscopy

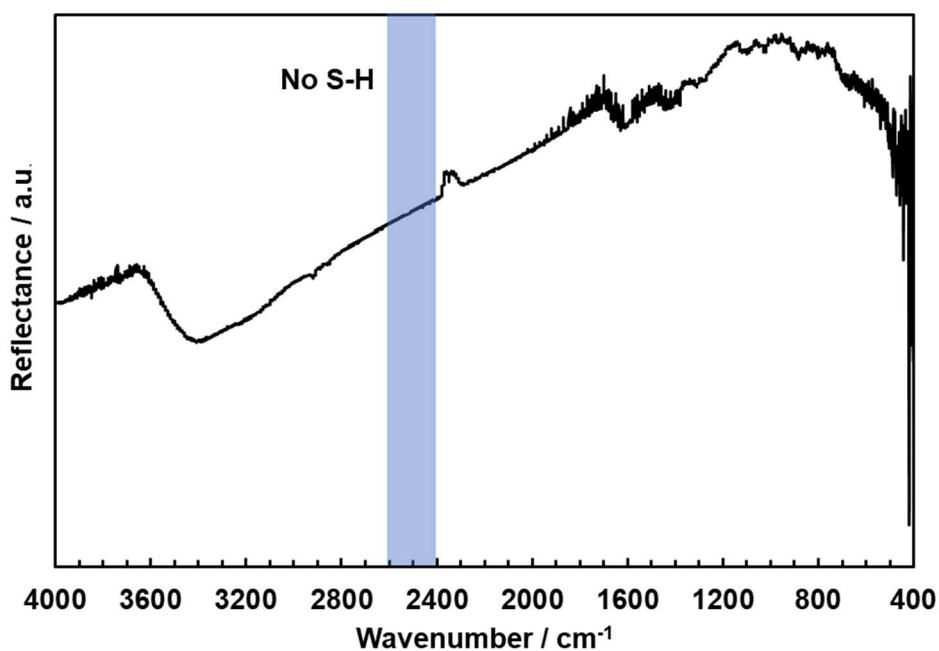


Figure 3-6. Infrared spectrum of **1-H**.

Infrared spectroscopy analysis of **1-H** shows the absence of a peak at around 2500 cm⁻¹ which indicates that the thiol groups of BHT have participated in the coordination reaction with Fe (II) ions (Fig. 3-6).

3.3.5. UV-Near Infra-Red (UV-NIR) Spectroscopy

UV-NIR spectroscopy reveals that **1-H** absorbs strongly in the UV region, with a peak at 295nm together with a weak and broad peak at around 1050nm.

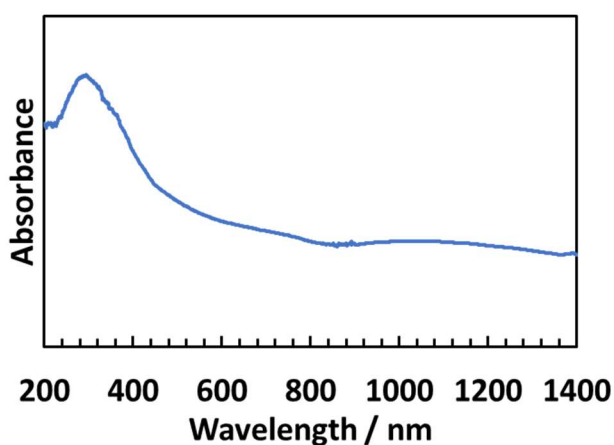


Figure 3-7. UV-NIR spectrum of **1-H**

3.4. Powder X-Ray Diffraction Studies and Simulations

Powder X-ray diffraction study of **1-H** was carried out to determine the structure of **1-H**. For comparison, synthesis of 1-RT was performed to understand how the temperature may affect the crystallinity of **1**. By the naked eye, it could be observed that **1-H** appeared more lustrous than 1-RT, a consequence of improved crystallinity in **1-H**.

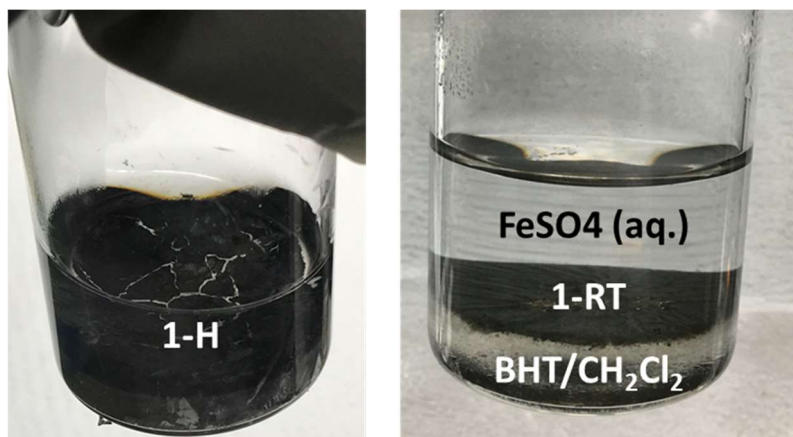


Figure 3-8. Optical photos of interfacial reactions of **1-H** (left) and 1-RT (right).

PXRD measurements reveal that **1-H** indeed possesses improved crystallinity compared to 1-RT, with the appearance of a few broad peaks in the PXRD pattern (Fig. 3-9). The PXRD pattern of **1-H** is very similar to that of the Type 2 metalladithiolene structure typical of CuBHT. Comparing PXRD patterns of **1-H** and CuBHT, it is observed that although the general topography of both spectra are similar, the (100) and (001) peaks are slightly shifted between CuBHT and **1-H**, as a result of their slightly different unit cell dimensions (Fig. 3-9).

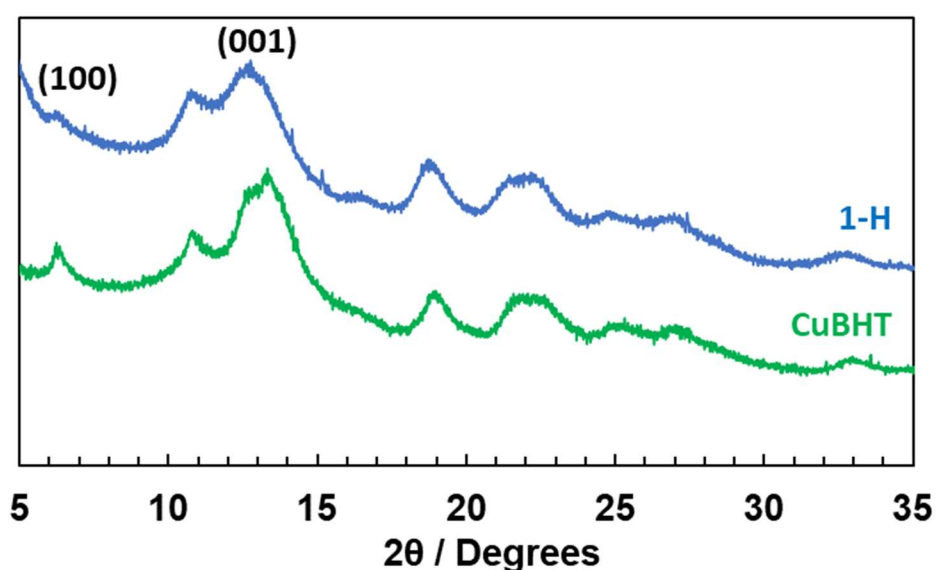


Figure 3-9. Powder XRD patterns of **1-H** and CuBHT.

From the PXRD pattern of **1-H**, the (100) peak at 6.35° gives an in-plane unit cell length of $a = b = 0.84$ nm and the (001) peak at 12.75° implies an interlayer d-spacing of $c = 0.36$ nm (Fig. 3-12). Three different configurations of interlayer stacking (AA stacked, AB stacked and AB slipped) were modelled, using a Type 2 hexagonal unit cell, with unit cell parameters $a = b = 0.84$ nm, and interlayer distance of 0.36 nm (Fig. 3-11). Of the three configurations, the AA stacked configuration matches most closely to that of the experimental **1-H** PXRD pattern (Fig. 3-10).

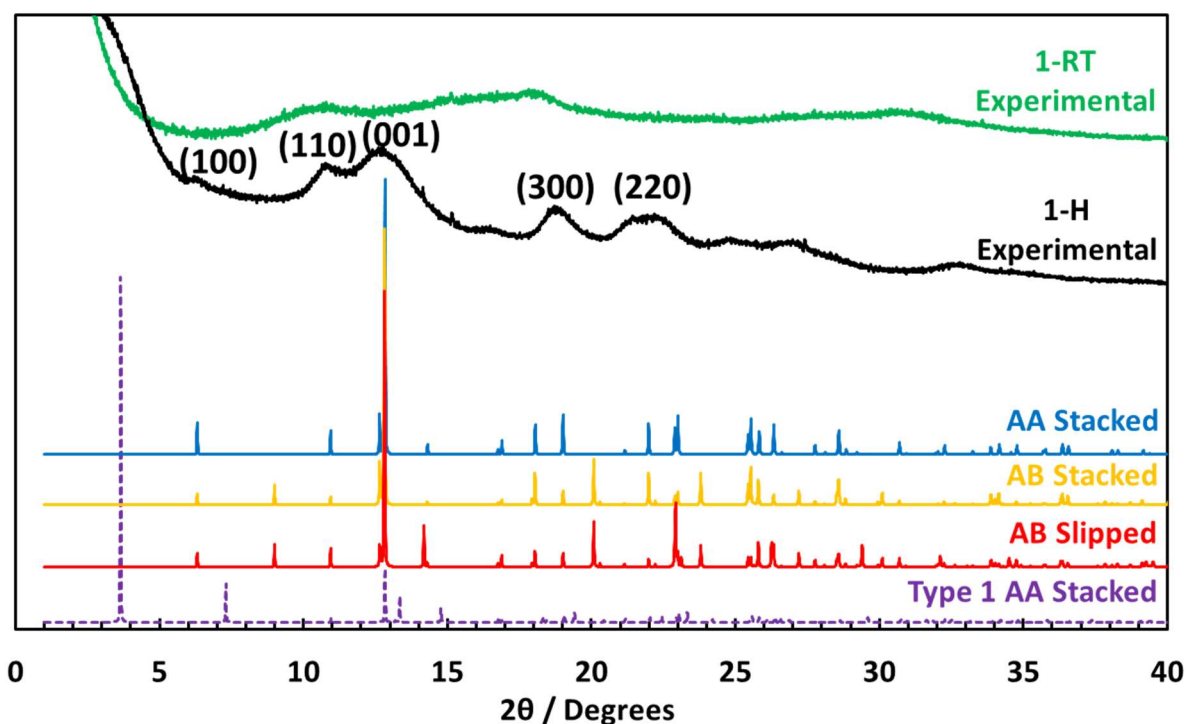


Figure 3-10. Experimental powder XRD spectra of **1-RT** (green) and **1-H** (black), simulated spectra of AA stacked (blue), AB stacked (yellow), and AB slipped (red) structures of Type 2 Fe-BHT, and AA stacked Type 1 Fe-BHT (purple).

The Type 1 Fe-BHT eclipsed structure was also simulated for comparison, with unit cell parameters $a = b = 1.45$ nm and $c = 0.36$ nm. The Type 1 structure does not match with the experimental spectrum due to the (100) peak at 3.56° not being visible and the (200) peak at 7.31° being absent (Fig. 3-10). Hence, it is concluded that **1-H** does not possess the porous Type 1 structure.

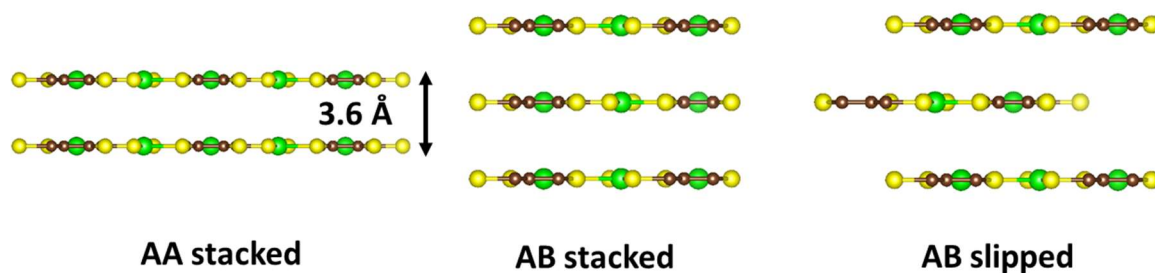


Figure 3-11. Side view of simulated stacking structures of **1-H**

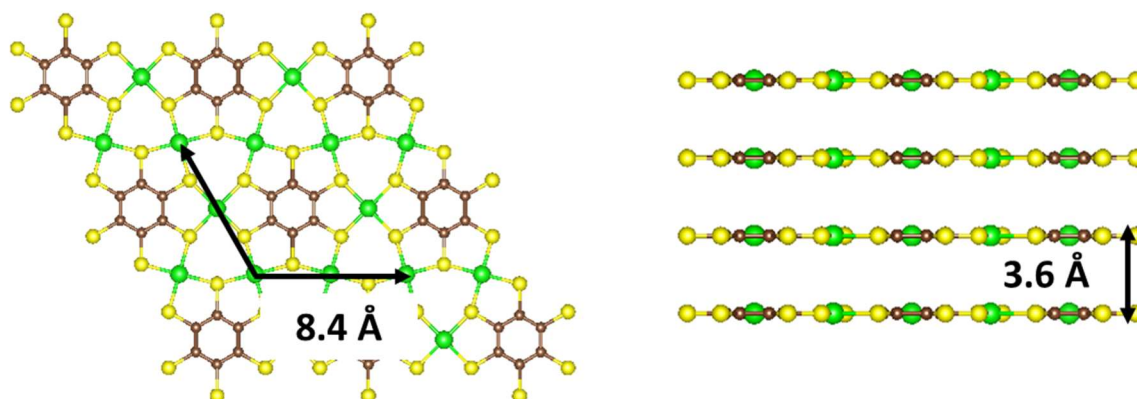


Figure 3-12. Top view (left) and side view (right) of multilayer **1-H** showing unit cell parameters.

Fast and random complexation between the Fe (II) ions and thiol groups, together with an energy barrier which needs to be overcome for structural rearrangement contribute to the lack of crystallinity in 1-RT compared to **1-H**. Improved crystallinity in coordination frameworks tends to impact the physical properties as well, hence it is important to compare how the physical properties have changed.

3.5. Electrical Conductivity Measurements

Electrical conductivities of **1-H** and 1-RT were measured and compared to understand the impact of improved crystallinity on conductivity. Thick nanosheets of **1-H** and 1-RT were scooped from the interfacial reaction mixture and deposited onto conductive Pt electrodes deposited on quartz glass (Fig. 3-13). AFM measurements of deposited **1-H** and 1-RT revealed thicknesses of 2.4 μm and 2.9 μm respectively (Fig. 3-14).

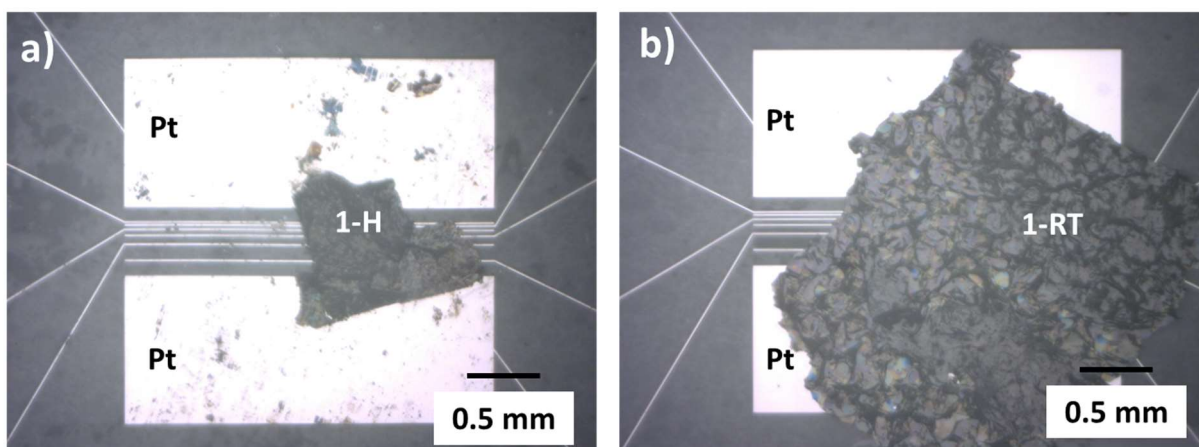


Figure 3-13. Optical photos of a) **1-H** and b) **1-RT** deposited on conductivity electrodes.

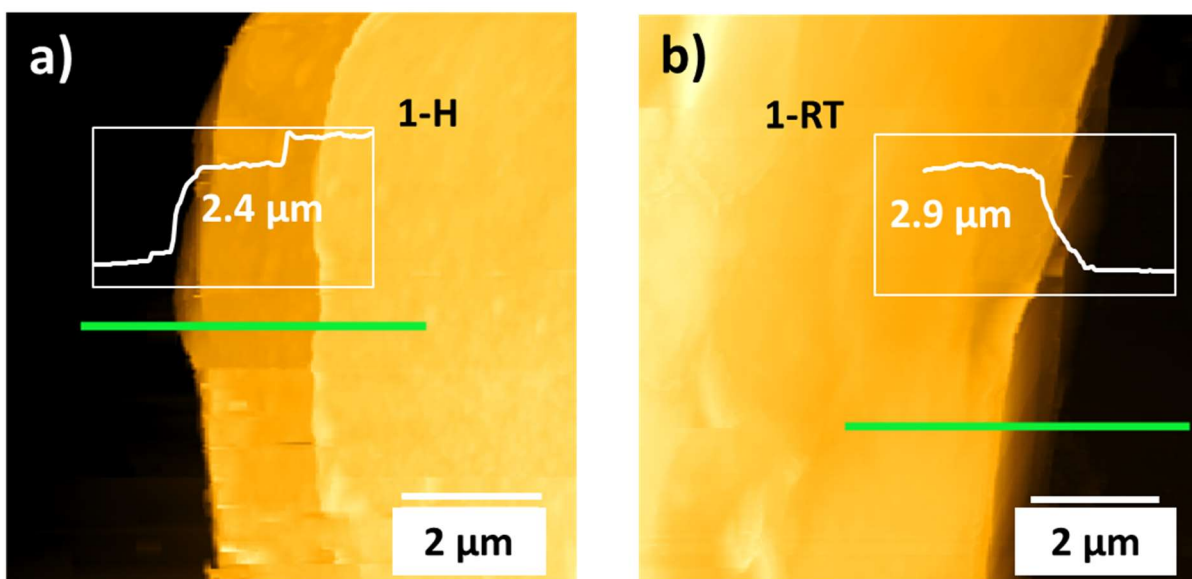


Figure 3-14. AFM micrograph of **1-H** and topography image (inset); (b) AFM micrograph of **1-RT** and topography image (inset).

Temperature dependent 4-probe conductivity was measured under argon from 298 K to 380 K. The conductivity at room temperature of **1-H** was 0.68 S cm^{-1} compared to 0.028 S cm^{-1} for 1-RT. Both **1-H** and 1-RT exhibit temperature dependence of electrical conductivity. Straight lines obtained while plotting the $\log(\text{conductivity})$ values against $1/T$ indicate that

thermally activated charge transport is involved.⁴ The Arrhenius law describes the activation energy required for thermally activated charge transport, as shown by the equation:

$$\sigma = A^{-E_a/kT}$$

where σ is the conductivity, A is an arbitrary constant, E_a is the activation energy, k is the Boltzmann constant and T is temperature (in Kelvin). The value of E_a was obtained by plotting $\log(\sigma)$ against $1/T$ and calculating the slope of the plot.

As the plots reveal, the improved crystallinity of **1-H** both lead to one order magnitude higher electrical conductivity and a lower activation energy barrier (270 meV for **1-H** compared to 360 meV for **1-RT**) for thermally activated charge transport compared to **1-RT** (Fig. 3-15). Improved crystallinity in coordination materials leads to larger domain sizes, effectively reducing the number of grain boundaries. In addition, lower defect density decreases the amount of scattering of mobile charge carriers, hence reducing the activation energy barrier.

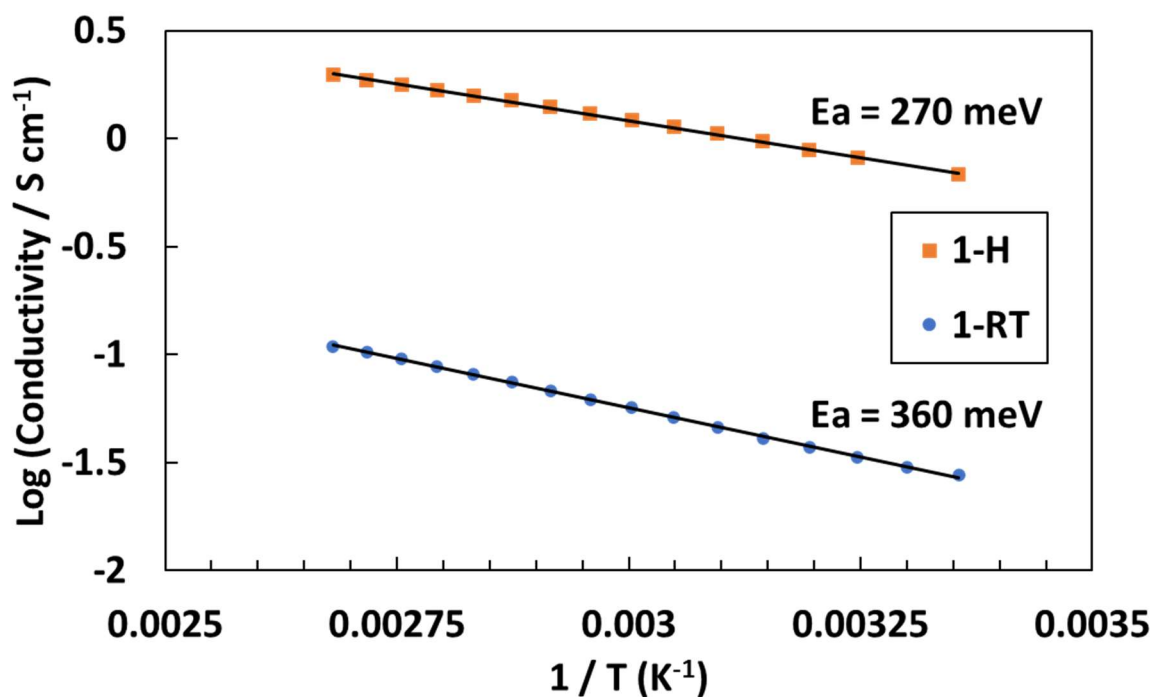


Figure 3-15. Log(conductivity) vs. $1/T$ plots and activation energies of **1-H** and **1-RT**.

3.6. Conclusion

The bisdithiolato iron(II) coordination nanosheet **1-H** was synthesized using a liquid-liquid interfacial reaction with heating. **1-H** was characterized with a variety of spectroscopies to shed light on its morphology, chemical bonding and structure. In particular, the higher crystallinity of **1-H** compared to 1-RT synthesized at room temperature was revealed by PXRD measurements. The structure of **1-H** comprises of planar 2-dimensional layers having a hexagonal Kagome lattice geometry with in-plane unit cell dimensions of 0.84 nm and AA stacked layers spaced 0.36 nm apart. Hence, **1-H** possesses the Type 2 structure like that of Cu-BHT⁵ (Fig. 3-16).

Conductivity measurements also showed that **1-H** has a semiconducting nature with room temperature conductivity of 0.68 S cm^{-1} and activation energy barrier of 270 meV. Elucidation of the chemical structure of the Fe-BHT nanosheet system together with a method of improving its crystallinity will enable further research in this material.

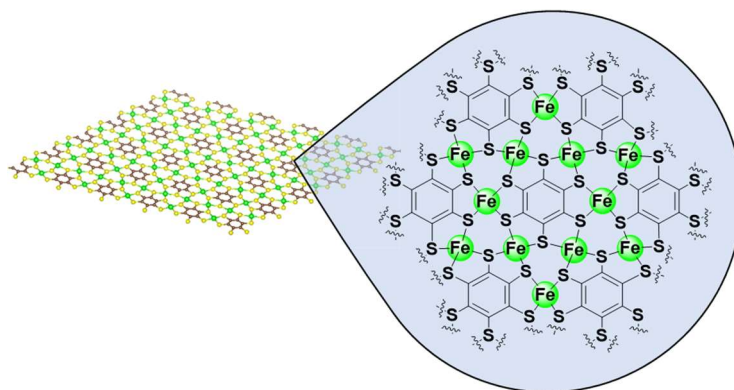


Figure 3-16. Chemical structure of the Fe-BHT nanosheet system.

3.7. Experimental

$\text{FeSO}_4 \cdot 7\text{H}_2\text{O}$, chloroform and ethanol were purchased from Kanto Chemical Co., Inc. Water was purified using the Milli-Q purification system (Merck KGaA). All solvents were degassed by purging with nitrogen before use. Benzenehexathiol (BHT) was synthesized according to the literature⁶. Silicon (100) wafers with 285 nm thermally grown oxide were purchased from Furuchi Chemicals, cut into desired size and sonicated with ethanol before use.

FE-SEM images were collected using a JEOL JSM-7400FNT equipped with an EDS analyzer (JEOL EX-2300). TEM images were recorded at 75 kV using a Hitachi HF-2000 equipped with an AMT-CCD camera. The TEM samples were prepared by depositing the respective nanosheets on a carbon film supported by a copper grid using an ethanol suspension. ATR-IR spectra were recorded using a JASCO FT/IR-6100 at room temperature under vacuum. XPS data were obtained using PHI 5000 VersaProbe (ULVAC-PHI, INC.). $\text{Al K}\alpha$ (15 kV, 25 W) was used as the X-ray source, and the beam was focused on a 100 mm^2 area. The spectra were analyzed with MultiPak Software and standardized using the C(1s) peak at 284.6 eV. AFM measurements were carried out using an Agilent Technologies 5500 Scanning Probe

Microscope, under ambient conditions, using the high-amplitude mode (tapping mode), with a silicon cantilever PPP-NCL (Nano-World). Powder X-ray diffraction data was obtained by synchrotron radiation ($\lambda = 0.8 \text{ \AA}$) at Beamline BL44B2 at Super Photon Ring-8 GeV (SPring-8) in Japan. To prepare the samples, **1-H** and **1-RT** were finely ground in an agate mortar and packed in 0.5 mm diameter soda tubes. UV-Vis spectra were taken using a JASCO V-570 spectrometer. Structural modelling and calculations were performed using Gaussian 09 package, and PXRD simulations were obtained using the VESTA program. SECCM measurements were conducted by collaborators (Assoc. Prof. Akichika Kumatani) at the Advanced Institute for Materials Research, Tohoku University.

3.7.1. Liquid-liquid Interfacial Syntheses

Synthesis of 1-H

In a glove box, 3.0 mg of BHT (0.011 mmol) was added to degassed chloroform (10 mL) at 45°C in a 50 mL glass vial of 40 mm diameter. Degassed pure water (10 mL) at 45°C was layered over the organic phase, and a solution of $\text{FeSO}_4 \cdot 7\text{H}_2\text{O}$ (11.6 mg in 0.5 mL water, 0.042 mmol) was added slowly dropwise into the aqueous phase. A thin black film developed at the interface within minutes, giving an opaque thick film after the reaction was left for 2 days at 45°C. After removing the aqueous and organic phases, thick **1-H** was washed thoroughly with water, chloroform and ethanol, and suspended in ethanol solution for further use.

Synthesis of 1-RT

In the glove box, 3.0 mg of BHT was added to degassed chloroform (10 mL) in a 50 mL glass vial of diameter 40 mm. Degassed pure water (10 mL) was then layered over the chloroform solution to form a double layer. A degassed aqueous solution of $\text{FeSO}_4 \cdot 7\text{H}_2\text{O}$ (10 mL, 5 mM, 0.05 mmol) was added cautiously to the aqueous layer. After 2 days, thick **1-RT** appeared at the liquid-liquid interface in the form of a black solid. After removing the aqueous and organic phases, thick **1-RT** was washed thoroughly with water, chloroform and ethanol, and suspended in ethanol solution for further use.

3.7.2. Temperature-dependent Electrical Conductivity Measurements

1-H and **1-RT** were deposited on quartz glass substrates with interdigitated Ti/Pt electrodes (No. 011598) purchased from BAS Co. Ltd. The samples were left to dry for 1 h under Ar, then vacuumed for 1h and transferred into a glovebox. The 4-probe conductivity measurements were performed using W tips (purchased from Micromanipulator Co. Ltd.) connected to a Keithley 2450 Sourcemeter. Measurements were conducted from 298 K to 380 K, under argon, and temperature control was achieved using a hot chuck controller (model DC-1260-P) connected to Si diode. The 4-probe measurement setup consisting of micromanipulators mounted on a measuring table placed on top of an anti-vibration stage and the entire setup enclosed in a glovebox, was custom ordered from Oyama Co. Ltd.

3.8. References

- (1) Dong, R.; Zhang, Z.; Tranca, D. C.; Zhou, S.; Wang, M.; Adler, P.; Liao, Z.; Liu, F.; Sun, Y.; Shi, W.; Zhang, Z.; Zschech, E.; Mannsfeld, S. C. B.; Felser, C.; Feng, X. *Nat. Commun.* **2018**, *9*, 2637.
- (2) Dong, R.; Han, P.; Arora, H.; Ballabio, M.; Karakus, M.; Zhang, Z.; Shekhar, C.; Adler, P.; Petkov, P. St.; Erbe, A.; Mannsfeld, S. C. B. B.; Felser, C.; Heine, T.; Bonn, M.; Feng, X.; Cánovas, E. *Nat. Mater.* **2018**, *17*, 1027.
- (3) Downes, C. A.; Clough, A. J.; Chen, K.; Yoo, J. W.; Marinescu, S. C. *ACS Appl. Mater. Interfaces* **2018**, *10*, 1719.
- (4) Mei, Y.; Diemer, P. J.; Niazi, M. R.; Hallani, R. K.; Jarolimek, K.; Day, C. S.; Risko, C.; Anthony, J. E.; Amassian, A.; Jurchescu, O. D. *Proc. Natl. Acad. Sci. U. S. A.* **2017**, *114*, E6739.
- (5) Huang, X.; Sheng, P.; Tu, Z.; Zhang, F.; Wang, J.; Geng, H.; Zou, Y.; Di, C.; Yi, Y.; Sun, Y.; Xu, W.; Zhu, D. *Nat. Commun.* **2015**, *6*, 7408.
- (6) Harnisch, J. A.; Angelici, R. J. *Inorganica Chim. Acta* **2000**, 300–302, 273.

Chapter 4

Fabrication and Transmetallation of Thin Bisdithiolatozinc(II) Nanosheets

本章については、5 年以内雑誌等で刊行予定のため、非公開。

Chapter 5

Lateral Heterojunctions by Transmetallation of Zinc(II) Dithiolene Nanosheets

本章については、5 年以内雑誌等で刊行予定のため、非公開。

Chapter 6

Conclusion and Perspective

本章については、5 年以内雑誌等で刊行予定のため、非公開。

Acknowledgements

The PhD journey leading up to this thesis was not one that I could have made alone, and hence I would like to express my gratitude to those who have been with me throughout this period:

First, I give all glory to God and the Lord Jesus Christ, whose divine provision, guidance and support have led me through the highs and accompanied me through the darkest times.

I am deeply indebted to Professor Dr. Nishihara Hiroshi, who has been a kind mentor and a very supportive supervisor both in research and in my life. I am grateful to his patience despite my many failings and giving me a nurturing space to grow as a researcher. I am honored to belong to his group.

I also am very grateful to Prof. Tetsuya Hasegawa for his help in organizing the defense committee, assisting in all the changes in paperwork and encouraging words throughout our interactions and discussions.

I am very thankful to Asst. Prof. Hiroaki Maeda, Asst. Prof. Naoya Fukui and Asst. Prof. Kenji Takada for their valuable scientific input many times when I get stuck. Special thanks also to Dr. Nagashima Sayoko, Dr. Wu Kuo Hui, Dr. Mariko Miyachi for their technical help when I faced problems.

I deeply appreciate the help extended to me from collaborators: Assoc. Prof. Akichika Kumatani and Mr. Sato Atsuki for the wonderful results of SECCM measurements measured in such short time frame; Prof. Kazuhito Tsukagoshi for his valuable research input; Prof. Sono Sasaki for her help in SPring-8 diffraction experiments.

I appreciate Assoc. Prof. Tetsuro Kusamoto for his kind directions in research; Assoc. Prof. Ryota Sakamoto and Assoc. Prof. Yoshinori Yamanoi for interactive discussions about life in general.

A big thank you to past lab members of Nishihara laboratory at the University of Tokyo Hongo Campus (from 2014 to 2020) which would be too long to list here. Throughout the many years of my research you have been a wonderful source of support and positive vibes in the laboratory and I will not forget the times we spent together in nomikais or summer camps.

I am indebted to the Japanese government for offering me the Monbukagakusho scholarship throughout my graduate study, without the financial help I would never have embarked on this journey in Japan.

I am thankful to exchange students Mami Horikawa and Martin Hoglund, for their help in my research and precious memories both in and out of research.

I am grateful for close partners in research Dr. Tigmansu Pal and Dr. Selezneva Ekaterina for insightful discussions into various aspects of this huge research field. I especially treasure the times of getting together and just sharing our thoughts on life, and also all the tea breaks! Special mention to Dr. Tigmansu Pal who has been a constant source of support, laughs, Indian food, snowboard partner which made this journey all the more memorable.

My friends in Singapore whose warm presence and constant visits (before the Covid pandemic) drove away the loneliness and distance I feel being here in Japan. Thank you to Eunice Phua Jia Han, Xiaozhi Lim, Yap Aik Heng, Ng Geck Woon, Ang Woo Tien, Reynard Lye, Colin Lim, Yeo Wee Hong, Lin Yan, Lim Siting, Goh Chin Siong and I miss you all.

A very special thank you to Brother Andrew Liao and Maureen Ma, spiritual mentors for your constant prayers and encouragements when I faced self-doubts and was not sure what to do with my life. Your words meant a lot to me.

Last but not least, my deepest gratitude to my family for their unflagging love and unconditional support throughout this journey: to my father Mr. Tan Ka Ong and my mother Mrs. Lee Siu Ling who let me walk this unique path. To my sister Tan Yan Cheng who has been taking on the burden of caring for my parents in my absence.

Finally, to my one and only life partner, Ms. Candy Zhang Xiaotong, who knew full well what she was getting into and still chose to marry me. Thank you for cheering me up and encouraging me in those difficult times, you are indeed God's blessing in my life.

Tan Choon Meng
University of Tokyo
June 2021

【Publication(s) related to the thesis】

1. “Determination of Chemical Structure of Bisdithiolatoiron Nanosheet” Tan, C. M.; Horikawa, M.; Fukui, N.; Maeda, H.; Sasaki, S.; Tsukagoshi, K.; Nishihara, H. *Chem. Lett.* **2021**, *50*, 576.

【Publication(s) not related to the thesis】

1. "Interfacial transmetallation synthesis of a platinadithiolene nanosheet as a potential 2D topological insulator" Pal, T.; Doi, S.; Maeda, H.; Wada, K.; Tan, C. M.; Fukui, N.; Sakamoto, R.; Tsuneyuki, S.; Sasaki, S.; Nishihara, H. *Chem. Sci.* **2019**, *10*, 5218.